RESEARCH ARTICLE

ADVANCED
MATERIALS
INTERFACES
Open Access
www.advmatinterfaces.de

Poly(L-Lactic Acid) Nanofiber-Based Multilayer Film for the Electrical Stimulation of Nerve Cells

Fengying Jiang, Yizhu Shan, Junyuan Tian, Lingling Xu, Chaohai Li, Fang Yu, Xi Cui, Chengwei Wang, Zhou Li,* and Kailiang Ren*

Poly(L-lactic acid) (PLLA) films have excellent piezoelectric properties, but the strong hydrophobicity of the surface makes it difficult for cells to attach there. PLLA nanofibers have good biocompatibility, but the weak piezoelectric coefficient limits the ability of the nanofibers to stimulate cell growth. Therefore, the PLLA piezoelectric film is combined with the PLLA nanofibers to make a multilayer film. In our tests, the piezoelectric output of the multilayer film ≈260 mV. In the biological experiments section, without piezoelectric stimulation, the cell length on the nanofibers is approximately twice that of the cells in the blank control group. The length of cells cultured on piezoelectric-based stimulated nanofibers is more than twice that of cells cultured on nanofibers without piezoelectric stimulation. Therefore, it is confirmed that under the dual action of nanofiber guidance and piezoelectric stimulation, the growth rate of cells is four times faster than that in ordinary Petri dishes. Intracellular calcium imaging experiments confirmed that the concentration of Ca^{2+} in electrically stimulated cells is approximately twice that of ordinary cells. It is also confirmed that piezoelectric materials can complete electrical stimulation of cells in indirect contact with cells.

1. Introduction

Tissue engineering utilizes known knowledge to improve the repair process of tissue in vivo or cellular products in vitro.[1–3] Because of the response to electrical stimuli in tissues, external electrical stimulation has been widely used to treat cell injuries and neurodegenerative diseases.[4,6] Electrical stimulation can be realized using several approaches, including electric current stimulation, triboelectric stimulation, and piezoelectric stimulation.[7,8] Distinguished from direct electrical stimulation using direct current (DC) or alternative current (AC), piezoelectric materials can directly stimulate the cell surface via material deformation, which is compatible with the human body.[4,8] Hence, developing piezoelectric materials with good biocompatibility and piezoelectric stimulation effects is crucial.

Poly(vinylidene fluoride) (PVDF)-based piezoelectric polymers have been widely employed in many applications, including sensors, and transducer and energy harvesting devices, because of their large piezoelectric coefficients, high impedance matching with the environment, and ease of processing.[10–14] Over the last decade, researchers have found that by using electrospinning methods, piezoelectric PVDF nanofibers can be produced with high piezoelectricity.[15,17] Therefore, significant research effort has been devoted to using electrospun PVDF nanofibers for applications in tissue engineering.[18] In 2018, Wang et al. (who are part of our research group) found that the electrospun PVDF-TrFE nanofiber-based scaffold showed good cell compatibility and a relatively large piezoelectric effect.[19] The proliferation rate of fibroblast cells cultured on the PVDF-based nanofibers increased by ≈1.6 times. In 2019, Maria Kitsara et al. attempted to use nanofibrous PVDF scaffolds to stimulate the growth of osteoblast cells. They found that the cell concentration on PVDF-based nanofibrous scaffolds was ≈9 times that of the control group.[20] However, the nonbiodegradability of PVDF materials limits their biomedical-related applications.

Because of their biocompatibility, relatively large piezoelectricity, and temperature stability, poly(lactic acid) (PLA)-based piezoelectric polymers have been widely used in biosensors, artificial blood vessels, artificial cartilage and other tissue engineering fields.[21] In 2018, Xia et al. modified the surface of

F. Jiang, C. Li, F. Yu, Z. Li, K. Ren
Center on Nanoenergy Research
School of Physical Science and Technology
Guangxi University
Nanning 530004, P. R. China
E-mail: zli@binn.cas.cn; renkailiang@binn.cas.cn
Y. Shan, J. Tian, L. Xu, X. Cui, C. Wang, Z. Li, K. Ren
Beijing Institute of Nanoenergy and Nanosystems
Chinese Academy of Sciences
Beijing 100083, P. R. China
Y. Shan, J. Tian, X. Cui, C. Wang, Z. Li, K. Ren
School of Nanoscience and Technology
University of Chinese Academy of Sciences
Beijing 100049, P. R. China
L. Xu
CAS Key Laboratory for Biomedical Effects of Nanomaterials
and Nanosafety and CAS Center for Excellence in Nanoscience
National Center for Nanoscience and Technology
Beijing 100190, P. R. China

The ORCID identification number(s) for the author(s) of this article can be found under https://doi.org/10.1002/admi.202202474.

electrospun PLLA nanofiber scaffolds and found that the modification significantly improved angiogenesis and nerve repair in rats.[22] In 2019, Gilbert et al. showed that rough and porous PLLA nanofibers were more conducive to the growth of dorsal nerve cells and arrangement of the axons along the fiber direction.[23] In addition, electrospun PLLA fibers showed a relatively low piezoelectric coefficient ($d_{14} \approx 2.3$ pC/N), which is much lower than that of stretched PLLA films ($d_{14} \approx 10$ pC/N).[24,25] Therefore, in this application, we combined PLLA nanofibers (NFs) with a PLLA thin film to prepare the multilayer structure of PLLA NF/PLLA film (PNFF). The pi ezoelectric properties, fiber uniformity, water contact angle and orientation of the PNFF structure were compared with the electrospun PLLA NFs and stretched PLLA film. Furthermore, the axonal outgrowth of rat pheochromocytoma-12 (PC-12) cells on the multilayer film was tested for cell elongation and proliferation. This result was also compared with the blank control group and other experimental groups.

2. Results and Discussion

2.1. Surface Morphology of Nanowires

The surface morphology of the PLLA nanofibers was examined using a scanning electron microscope (SEM) (SU 8020, Tokyo, Japan), and the images are shown in **Figure 1**. As the solution concentration of the PLLA solution was increased from 6% to 9% (all concentrations in this investigation are represented as wt.%), the average sizes of the PLLA nanofibers were increased from 600 to 1500 nm (Figure 1a–c). The reason is the increasing viscosity of the PLLA solution at high concentrations, in which the polymer solution overcomes more force to be split to a smaller size during the electrospinning process.[23] As shown in the SEM images in Figure 1b, the nanofibers showed excellent uniformity when the solution concentration was 7.5%. The

gap distance can largely affect the crystallinity, alignment, and piezoelectric properties of the PLLA nanofibers.[27] Therefore, the effect of the gap distance on the surface morphology of the PLLA NFs was assessed, such as gap distances of 15 cm, 20 cm, and 25 cm. As shown in the SEM images (Figure 1d–f), the PLLA NFs partially diffused and twisted together slightly. The reason may be the unevaporated solvent on the PLLA NFs after the electrospinning process due to the short gap distance. When the gap distance increased to 20 cm (Figure 1e), the PLLA NFs became uniformly distributed with fiber sizes of ≈700 nm. With the increasing gap distance to 25 cm, the PLLA fibers become randomly distributed (Figure 1f). Therefore, the optimized conditions for electrospun PLLA fibers were chosen as a 7.5% solution concentration and a gap distance of 20 cm. In addition, The expansion of water contact angle was not conducive to cell attachment.[28] The water contact angle of the PLLA nanofibers was measured (Figure S1, Supporting Information). The water contact angle was slightly increased to 85.1° for the PLLA NFs produced with a 7.5% PLLA solution.

2.2. Crystallization Analysis

Differential scanning calorimetry (DSC, Mettler Toledo LLC, OH, USA) can be used to measure the enthalpy of materials, and the data are shown in **Figure 2**a. The DSC data of the annealed PLLA film showed only one melting peak (T_m) at ≈169 °C that slowly increased with increasing annealing temperature. In addition, the crystallinity of the PLLA was calculated using the equation below.
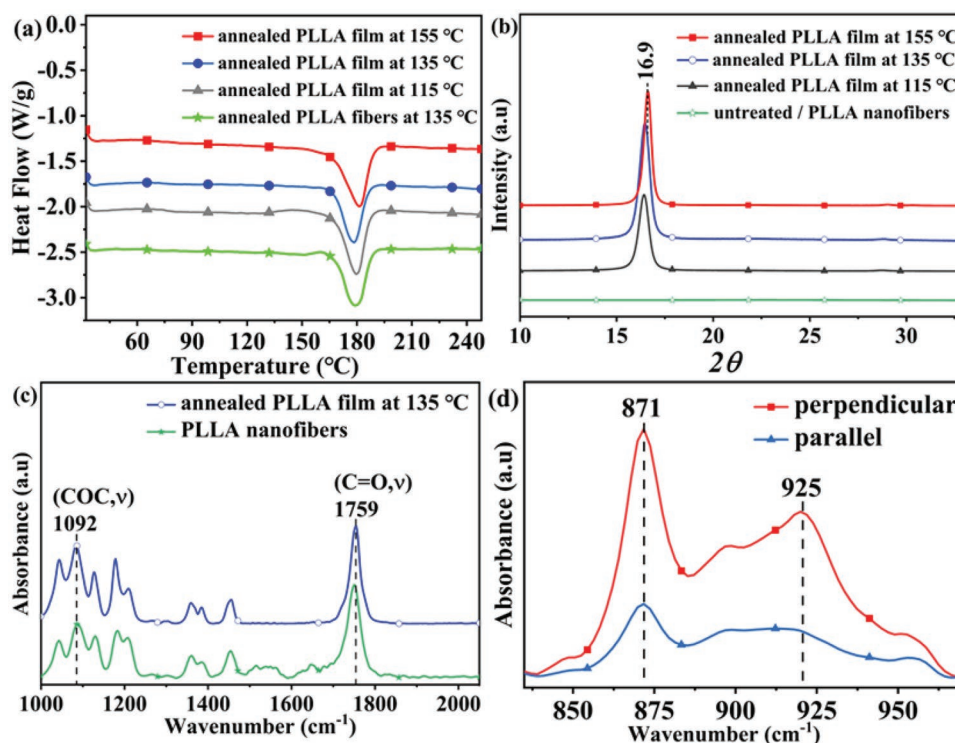
$$x = \left(\frac{\Delta H_m}{\Delta H_f} \right) \times 100\% \tag{1}$$

where ΔH_f represents the melting enthalpy of the PLLA films with 100% crystallization, and ΔH_m is the melting enthalpy
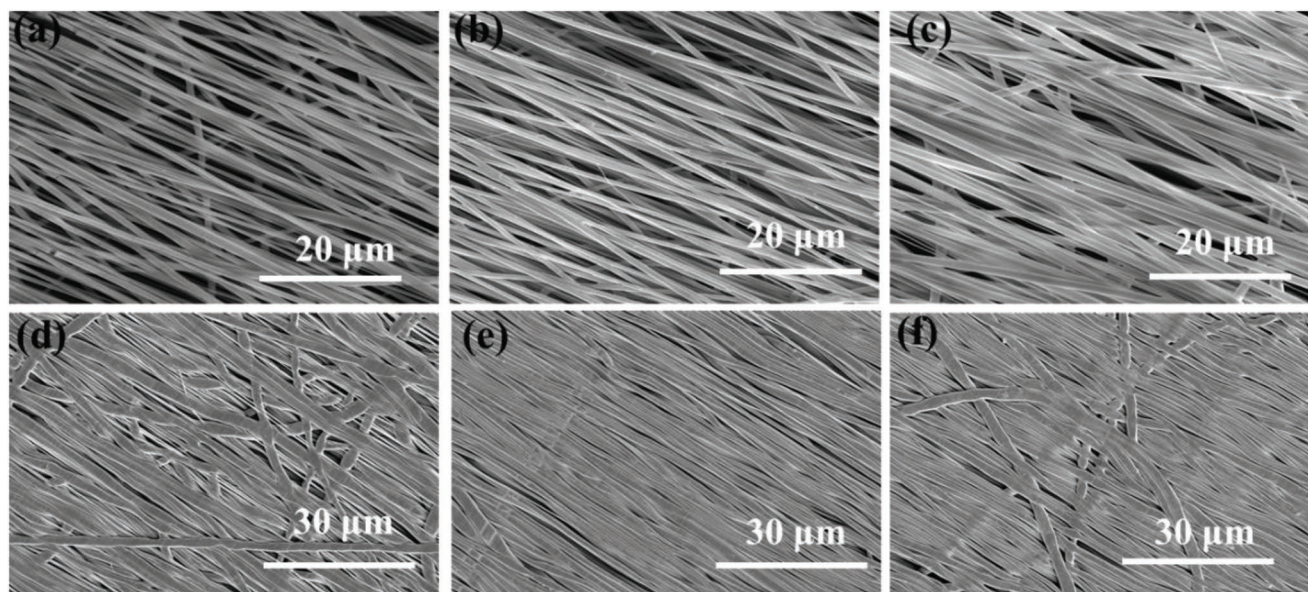
Figure 1. SEM images of PLLA nanofibers fabricated using various solution concentrations and gap distances: a) 6%, 20 cm; b) 7.5%, 20 cm; c) 9%, 20 cm; d) 7.5% 10 cm; e) 7.5%, 15 cm; f) 7.5% 25 cm.

**ADVANCED
SCIENCE NEWS**

www.advancedsciencenews.com

**ADVANCED
MATERIALS
INTERFACES**

www.advmatinterfaces.de

Figure 2. a) differential scanning calorimetry (DSC) of PLLA nanofibers (annealed at 135 °C) and PLLA films annealed at various temperatures. b) X-ray diffraction (XRD) patterns. c) Fourier transform infrared (FTIR) spectra of PLLA films and nanofibers. d) Polarized FTIR spectra of annealed PLLA film at 135 °C measured using the polarized incident beam along the parallel and perpendicular directions of the stretching direction.

of the PLLA film.[29] From the data, the crystallinity increased with increasing annealing temperature. As the calculated result shows in **Table 1** (in the supporting information). The crystallinity of the PLLA film increased with increasing annealing temperature, and the PLLA nanofibers showed the lowest crystallinity. The highest crystallinity reached 60% for the film annealed at 155 °C. However, the increased temperature also increases the brittleness of PLLA films.[30] Therefore, 135 °C was chosen as the annealing temperature for the remaining of the investigation.

Figure 2b shows the XRD patterns of annealed PLLA film with various annealing temperatures and annealed PLLA film. The diffraction peak at 2θ of 16.9° (110/200, α phase) of the annealed PLLA film was much higher than that of the PLLA nanofibers, indicating increasing crystallinity in the PLLA film.[31] The diffraction peak at 16.9° for the PLLA nanofibers was much smaller than that of the PLLA films. The annealing temperature markedly influenced the crystallinity of the PLLA material. With increasing annealing temperature, the crystal size increased gradually. The Fourier transform infrared (FTIR) spectra of the PLLA film and nanowires are shown in Figure 2c. The characteristic peaks at 1092 cm^{-1} and 1759 cm^{-1} are associated with C=O and −C−O−C− functional groups in a PLLA material. The piezoelectric property of the PLLA material arises from the polarization of C=O dipoles in the material.[25] Therefore, the increasing absorption peak at 1092 cm^{-1}corresponds to the increasing fraction of C=O groups, causing increased piezoelectricity in the PLLA film. Furthermore, to assess the alignment of the functional groups during the stretching
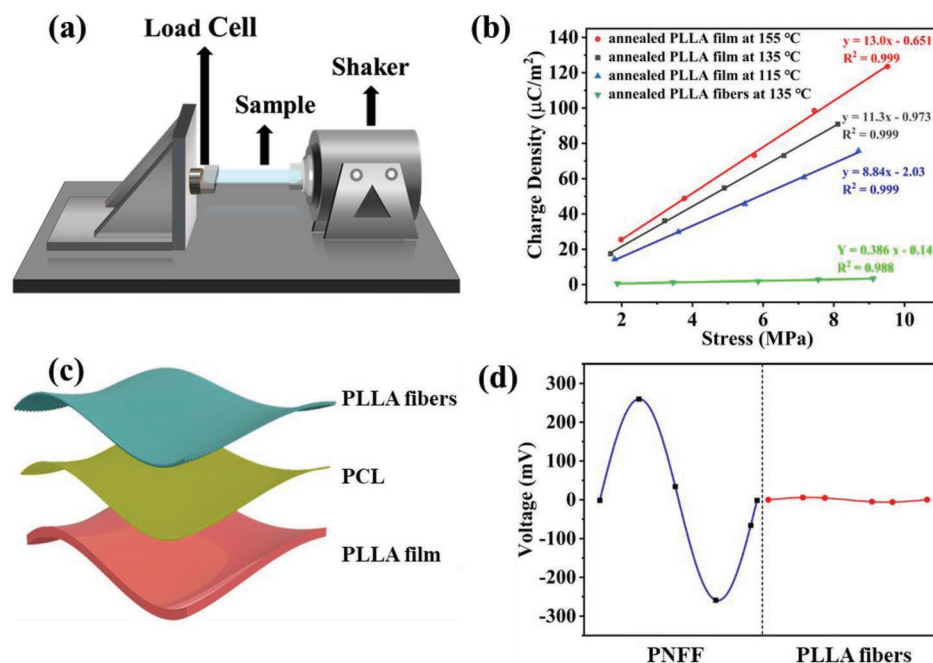
process, polarized infrared (IR) light was incited along the perpendicular and parallel directions of the stretching direction of the PLLA film.[32] The enlarged FTIR spectra between 871 and 960 cm^{-1} for the PLLA film are shown in Figure 2d. The characteristic peaks at 871 and 960 are much larger in the perpendicular direction than in the direction parallel to the stretching direction of the PLLA film. Previous literature has revealed that, C=O dipoles feature 125° with the main carbon chain of the PLLA film, and the vibration direction of C=O dipoles is mainly perpendicular to the stretching direction of the PLLA film. Therefore, most of the PLLA molecule chains are oriented parallel to the stretching direction after stretching.

2.3. Measurement of Piezoelectric Performance

Because of the 125° angles between the C=O dipoles and main carbon chain of the PLLA materials, the dipole component perpendicular to the main chain will cancel each other out, and only the component parallel to the main polymer chain can show polarity. Therefore, the PLLA film only showed piezoelectric properties along the d_{14} direction. The piezoelectric coefficient d_{14} of the PLLA film can be calculated using the equation below:

$$d_{14} = \frac{D_{sur}}{T_4} = \frac{Q_{sur}}{A_{sur}} \left(\frac{F}{A_{cro}} \right)^{-1} = \frac{A_{cro}}{A_{sur}} \cdot \frac{\int I dt}{F} \tag{2}$$

where D_{sur} is the surface charge density, T_4 is the applied stress along the shear direction, Q_{sur} is the generated surface charge,

ADVANCED
SCIENCE NEWS
www.advancedsciencenews.com

ADVANCED
MATERIALS
**INTERFACES**
www.advmatinterfaces.de

Figure 3. a) Schematic diagram of the piezoelectric coefficient measurement setup. b) Output charge as a function of applied stress for the PLLA films annealed at various temperatures. c) Schematic drawing of the PNFF multilayer film. d) Comparison of the output voltage of the PNFF film scaffold and PLLA nanofiber scaffold with an input voltage of 3 V at 10 Hz on the bottom speaker of the culture plates.

A_{sur} is the surface area, F is the applied force, A_{cro} is the cross sectional area, I is the current, and t is the time.[33] **Figure 3**A is A schematic diagram of an experimental apparatus for measuring piezoelectric coefficients. It mainly consists of a load cell, an SRS power amplifier, a phase-lock-in amplifier and a shaker. The lab-designed piezoelectric coefficient setup comprises a load cell, an SRS power amplifier, a phase-lock-in amplifier and a shaker (Figure 3a). The piezoelectric coefficients of the PLLA films with various annealing temperatures (115, 135, and 155 °C) were measured. The measurement results for the d_{14} of the PLLA film at various annealing temperatures are shown in Figure 3b. The d_{14} of the PLLA film slowly increased from 8.85 to 13.1 pC/N with increasing annealing temperature, indicating that the piezoelectric properties of the PLLA film slowly increased with the enhanced crystallinity. At the same time, we also performed a statistical error analysis of the piezoelectric coefficient (Figure S3a, Supporting Information). In addition, the stress–strain curve of the annealed PLLA film was measured, and the data are shown in Figure S3b in the supporting information. The film annealed at 155 °C was easily damaged with a lower force at 4% strain, a level much lower than that with the other PLLA films. The reason is mainly attributed to the increased brittleness of the film with increasing crystallinity. Therefore, as explained above, the PLLA film annealed at 135 °C was chosen for the remainder of the study. Piezoelectric fibers have been shown to benefit cell elongation along fiber directions.

Therefore, the PLLA nanofibers were glued to the top of the PLLA film using a low melting temperature polycaprolactone (PCL) nanofiber. A schematic drawing of the PLLA NFs/film (PNFF) multilayer film is shown in Figure 3c. The output performance of the PLLA NFs and PNFF multilayer film were measured, and the measurement results are shown in Figure 3d. The data indicate that the open circuit voltage of the PNFF film reached 200 mV, which is >90-fold higher than that of the electrospun PLLA NFs. Therefore, the output signal of the PNFF film mainly arises from the stretched PLLA film inside the multilayer PNFF film. The electrospun PLLA fibers were shown to benefit the elongation of fibroblast cells along the fiber direction. Therefore, the PNFF multilayer film was utilized for the remainder of the cell experimental process.

The schematics of the lab-designed flexible bottom culture plate are shown in **Figure 4**a. The culture plate comprises two thick acrylic plates (>5 mm in thickness), PNFF multilayer film, and a small speaker (Edifier Technology Inc., Guangdong, China). In the culture plate, two thickness acrylic pieces were drilled into a 35 mm hole in the middle, and the PNFF multilayer film was sandwiched between them as the base of the culture plate, which was then glued to a speaker using a thick double-sided glue (3 M Co. Ltd., MN, USA). Before the PNFF film was glued in the middle of the culture plate, Au electrodes (2 cm in diameter) were sputter coated on the top and bottom of the PNFF film as the active layer of the plate. Before testing the electric output of the culture plate, the culture plate was filled with saline solution to simulate the cell growth condition. The open circuit voltage (V_{oc}) of the device changed slightly with the frequency of the vibration signal (Figure 4b). This finding may be related to the resonance frequency of the speaker. The V_{oc} of the culture plate reached its maximum value of ≈1.5 V at an input voltage of 2 V at 50 Hz. Afterward, the V_{oc} of the culture plate was slightly increased to ≈2 V with an input signal of 3 V at 50 Hz (Figure 4c). Furthermore, with the increasing
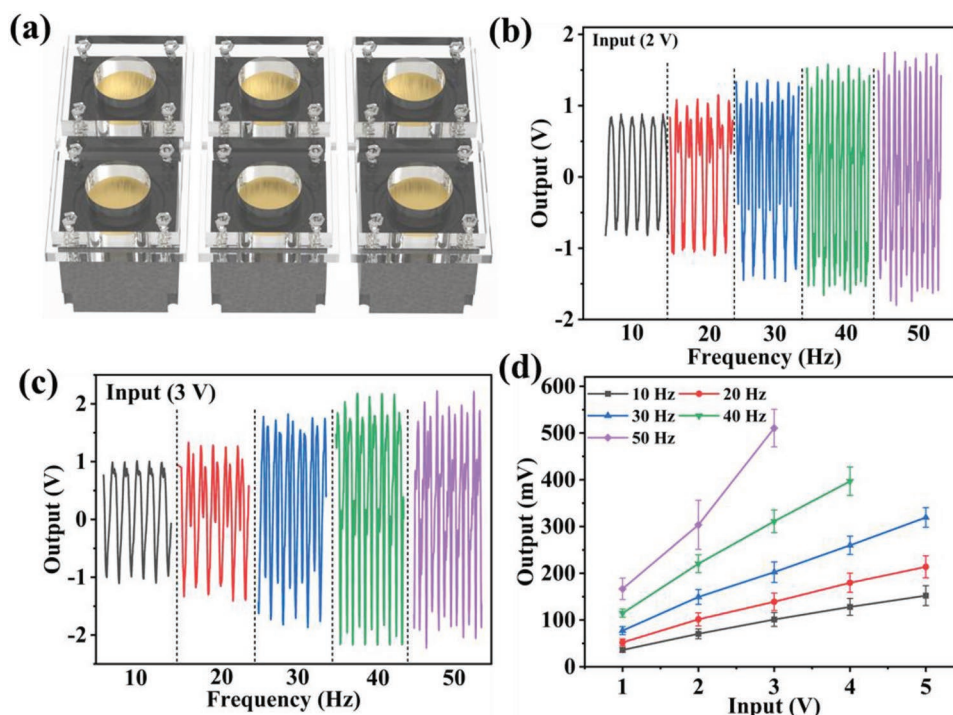
Figure 4. a) Schematic diagram of the lab-designed cell culture plate. Voltage output of the PNFF-based culture plates at different frequencies and input voltages: b) 2 V, 10–50 Hz. c) 3 V, 10–50 Hz. d) Output voltage of the PNFF-based culture plate as a function of input voltage on the bottom speaker at various frequencies, 10–50 Hz. Samples ≥ 15.

input signal, the vibration of the culture plate became very strong with increasing frequency, which may generate standing waves on the PNFF substrate and damage the cells on the culture plate. Therefore, an AC signal of 3 V at 50 Hz was chosen as the input signal to the speaker for the remainder of the cell experimental process (Figure 4d).

2.4. Biocompatibility Test

Biocompatibility is an important parameter to evaluate the compatibility of biomaterials with cells or living body.[34] This is the premise of whether the materials we choose can be used in biological systems. The state of cell viability and proliferation could reflect the toxicity of the materials. Biocompatibility can also provide a reliable reference for the future clinical application of this kind of biomaterials.[35] In this study, we used Live/Dead stain and Cell Count Kit-8 (CCK-8) test to evaluate the biocompatibility of the PLLA multilayer film.

For the live/dead stain, Calcein-AM is a cell staining reagent for fluorescence labeling living cells with green fluorescence (E_x = 490 nm, E_m = 515 nm). Once the reagent enters the cell, Calcein-AM (which does not fluoresce itself) is cleaved by intracellular esterases to form the membrane-impermeable polar molecule Calcein, then Calcein retained in the cell and emits strong green fluorescence. Due to the lack of esterases in dead cells, Calcein-AM is only used to label live cells. Propidium iodide (PI) could not pass through the cell membrane of living cells, but can only pass dead cell membranes to reach the nucleus and produce red fluorescence (E_x = 535 nm,

E_m = 617 nm). We cultured PC-12 cells on the multilayer film for up to five days and stained the cells of 1, 3, and 5 days. The viability of cells on the multilayer films and tissue cell plates showed no significant difference (**Figure 5**a,b). Live cells could react with CCK-8 reagent and produce orange precipitate – Formazan. The more living cells, the more Formazan produced and the darker the color. The absorbance of the cells at 405 nm on the multilayer films and tissue cell plates indicated no obvious differences at 1,3, and 5 days (Figure 5c).

2.5. Effect of Multilayer Films on Cell Differentiation and Growth

In this study, we chose PC-12 cells as the experiment cells. Which have the general characteristics of neuroendocrine cells, and are widely used in neurophysiological and neuropharmacological research.[37,36] The morphology of the rat pheochromocytoma (PC-12) cells on the PNFF multilayer films was first observed using SEM images (**Figure 6**a,b). Poly(lactic acid) (PLA) materials have been demonstrated to feature both a levo-(L) helical structure and dextral- (D) helical structure.[26] Therefore, PLA materials show nonpiezoelectric properties. However, Young's modulus and the chemical properties of PLA materials are similar to those of PLLA materials. Therefore, in the PC-12 cell test, the PLLA NFs were combined with a PLA film as one of the control groups. In the biocompatibility test of the PNFF film, PLLA nanofibers were glued on the nonpiezoelectric PLA film as a control group to compare with the PNFF film. Four experimental groups were set up as follows: i) blank control
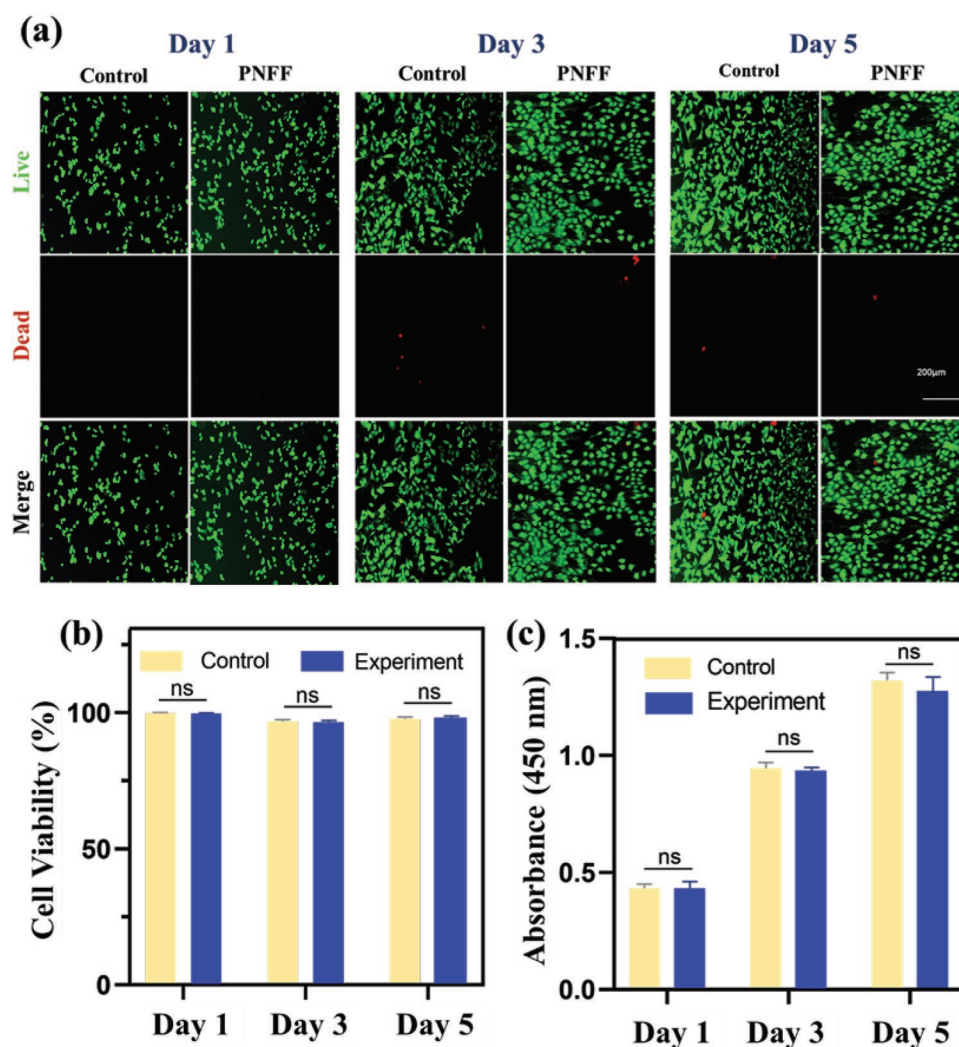
Figure 5. Cytobiocompatibility of the multilayer films. a) Live/dead staining of PC-12 cells on cell culture plates (control group) and fiber/PLLA films. b) The viabilities of PC-12 cells in the control and fiber/PLLA film groups were the same. c) PC-12 cell viability determined by the CCK-8 assay. ns: $p > 0.05$.

group; ii) PNFF film with no excitation, iii) PLLA NFs/PLA film with excitation at 50 Hz, ±3 V signal to the speaker, and iv) PNFF film with excitation of ±3 V at 50 Hz to the speaker. Immunofluorescence staining and SEM photographs were then performed to evaluate the cell morphology on different culture plates (Figure 6a).

The experimental results indicate that the PC-12 cells in the blank control group showed much less directionality than the PC-12 cells grown on the PLLA NF-based culture plates (Figure 6a). However, no significant difference was found in the directionality of PC-12 cells in the experimental groups with (group (iv)) or without piezoelectric stimulation (groups (ii) and (iii)). This finding indicates that the orientation of PC-12 cells mainly arises from the alignment of the PLLA nanofibers on the cell culture plate, which is not associated with piezoelectric stimulation. Furthermore, the differentiation rate and average neurite length of PC-12 cells in the experimental and control groups were calculated using confocal fluorescence microscopy (CFM), and the histogram results are shown in Figure 6c,d. The histogram results showed that the cell differentiation rate

in Group (IV) (with piezoelectric stimulation) was 41% higher than that in the control group (56.3%). (Figure 6c). Compared with the experimental group using the same culture plate, the cell differentiation rate of PC-12 cells in Group IV (with piezoelectric stimulation) was 11% higher than that without piezoelectric stimulation (Group ii). Even compared with the PLLA NFs/PLA scaffold with the same excitation, the differentiation rate in the PNFF scaffold film was 7.7% higher. This result indicates that the piezoelectric stimulation from the PNFF scaffold can substantially benefit the differentiation rate of PC-12 cells. The histogram results in Figure 6d showed that the average cell length of Group (iv) reached 142.76 µm, which is 4.15-fold and ≈2-fold that of the control group (34.37 µm) and other experimental groups (Group (ii): 70.2 µm; Group (iii): 65.6 µm), respectively. The experimental results of the groups (i) and (ii) showed that the surface morphology of the material would promote the growth of cells. But the effect is limited. The experimental results of the groups (ii) and (iii) showed that mechanical vibration did not promote the growth of cells. The experimental results of the groups (iii) and (iv) show that
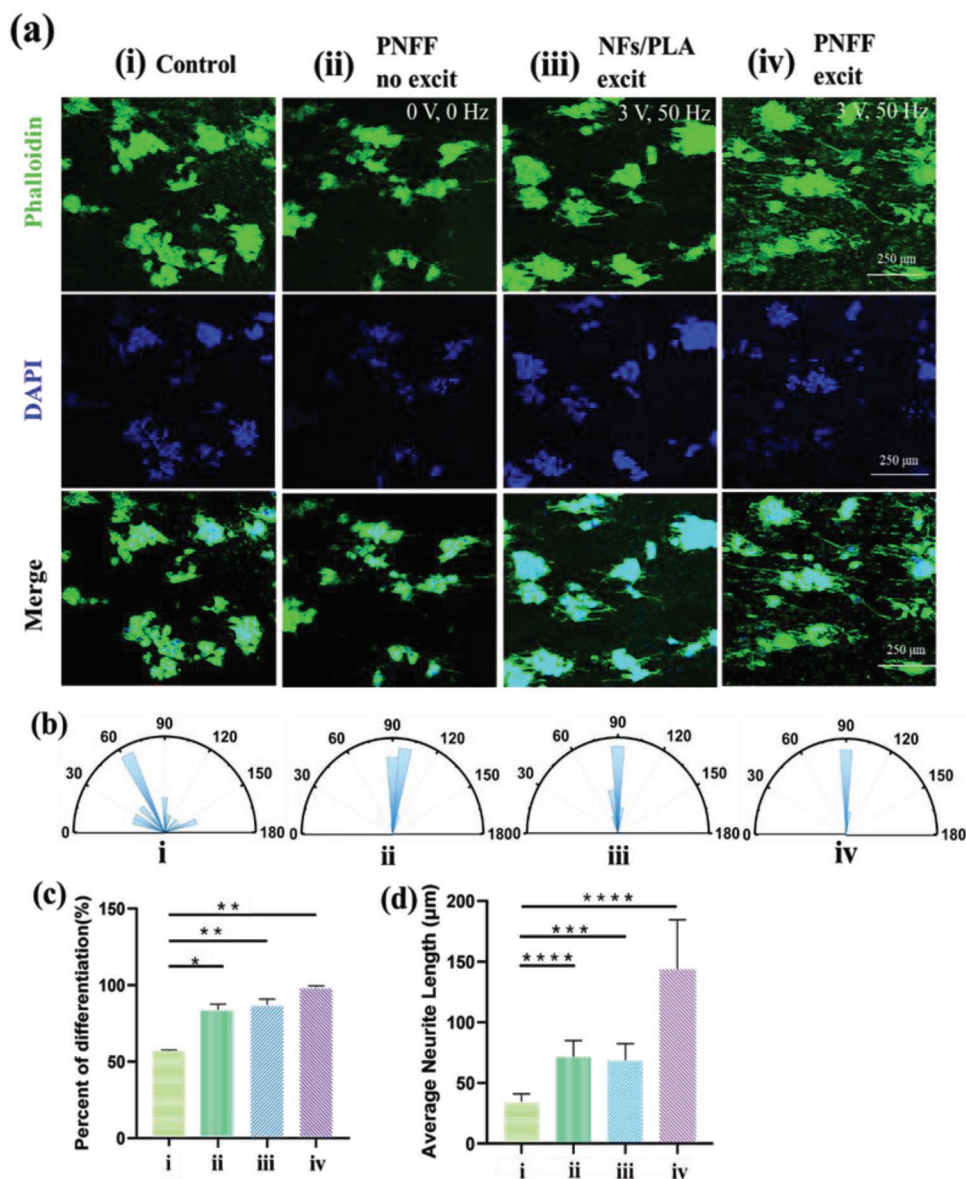
Figure 6. Growth results of PC-12 cells in different situations. a,b) SEM images of PC-12 cells aligned on the fiber/PLLA films. c) Fluorescence image of cellular filamentous actin (green) and nuclei (blue) of different groups. d) Corresponding angular histograms of cell nuclear angles from the results in (c). e) Statistical results of the percent of cell differentiation and average neurite length (μm). p values: [****]$p < 0.0001$, [***]$p < 0.001$, [**]$p < 0.01$ or [*]$p < 0.05$.

the growth of cells is mainly caused by the stimulation of cells by the charge generated on the surface of the PLLA film under vibration. This experimental process proved that the PNFF-based scaffold could generate electric signals, markedly improving the cell elongation and differentiation rate.

2.6. Intracellular Calcium Ion Level Test and the Gene Expression of Neurons

Calcium is a critical parameter that indicates the cellular responses to electrical stimulations, such as cellular metabolism, synaptic transmission, regulation of the cell cycle, and intracellular communication processes of neural cells.[38] The

Figure 7a showed the underlying molecular mechanism of the PC12 differentiation by PLLA piezoelectric stimulation. This kind of stimulation method could activate Ca^{2+} channel and promote calcium influx, then trigger downstream signaling pathway. The increased Ca^{2+} concentration activates calmodulin directly and leads to the activation of adenylyl cyclase (AC). Downstream pathways directly are regulated by cyclic adenosine monophosphate (cAMP) including the core gene protein kinase phosphokinase A (PKA) that activates this pathway. [39] To confirm that the cell growth and differentiation in this experimental process were excited by the piezoelectric stimulation from the PNFF film, the intracellular Ca^{2+} concentrations were measured using the calcium fluorescence staining method. In this method, once cells are combined with Ca^{2+} ions, the
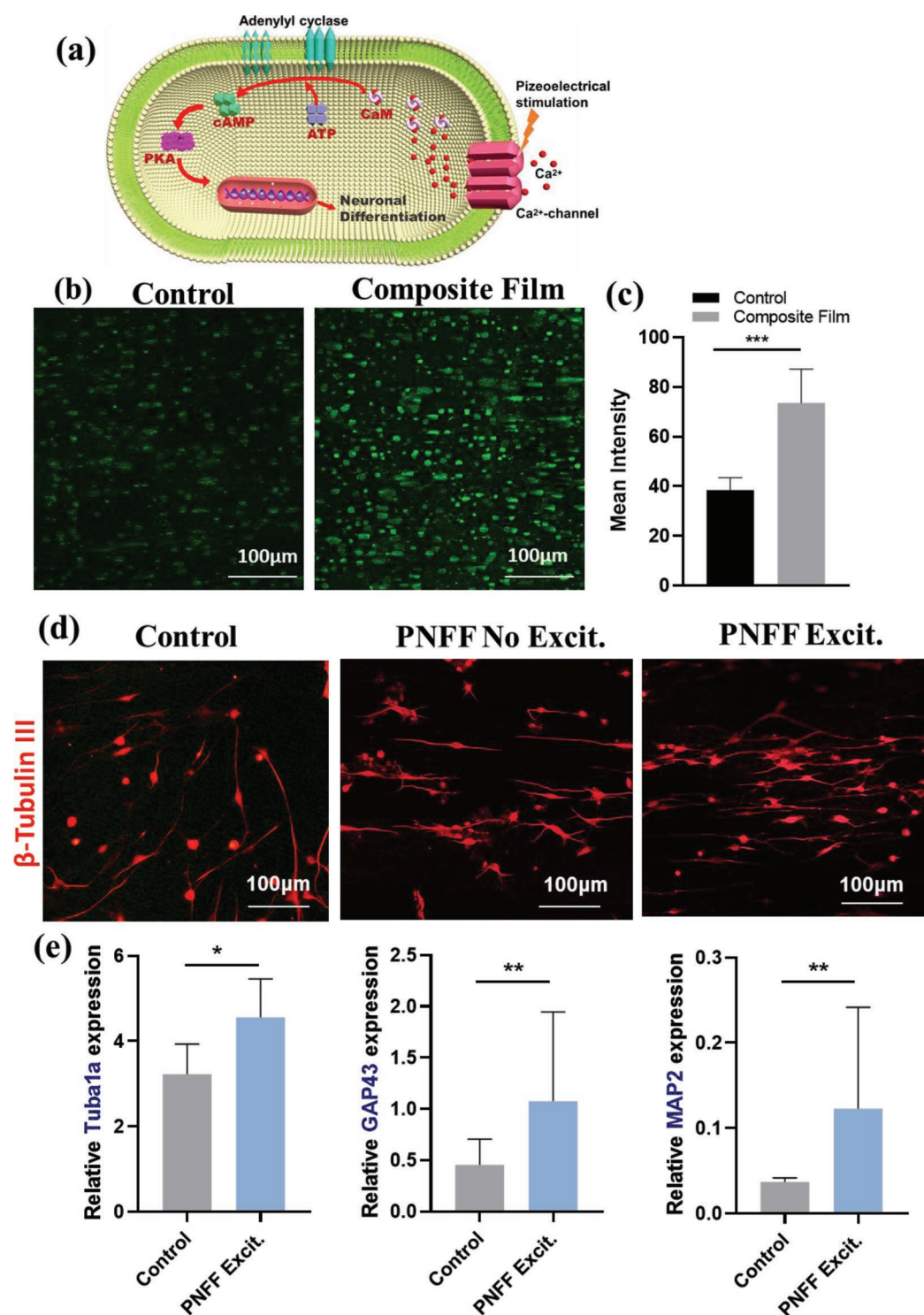
Figure 7. Intracellular Ca^{2+} level of PC-12 cells and The growth of primary neurons of rats under different conditions. a) Mechanism diagram of calcium ion promoting nerve cell growth under electrical stimulation. b) Confocal fluorescence images of PC-12 cells stained with Fluo-4 AM after piezoelectric stimulation for five days. c) Statistical graph of the mean fluorescence intensity acquired from the confocal photos. $n = 15$. d) Immunofluorescence staining of neurons, red β3- Tubulin positive cells. e) The expression of growth related genes Tuba1a, GAP43 and MAP2 expressed by neurons of control group and PNFF with excitation group.

fluorescent indicator can enter the cells with Ca^{2+} ions, and the concentration of Ca^{2+} ions can be detected according to fluorescence intensity. During the experimental process, Ca^{2+} ions

were stained using Flou4-AM (acetoxymethyl) ester for both the intracellular and extracellular fluids. During the experimental process, both the control and experimental groups utilized

the PNFF film as the scaffold film for the cell test. The control group was kept still without vibration, and the experimental group was subjected to vibration using a 3 V AC signal at 50 Hz. After five days of the piezoelectric stimulation process (2 h/time, 2 times/day), CFM images of the PC-12 cells were taken using a laser scanning confocal microscope (SP8, Leica, Germany), and the images are shown in Figure 7b. Experimental results showed that the Ca^{2+} concentration in the experimental group was much higher than that in the control group (Figure 7c), indicating that the piezoelectric stimulation in this study can open Ca^{2+} channels in cells and increase the intracellular Ca^{2+} concentration of PC-12 cells.

Although PC12 cells have been used as substitutes in many experiments for nerve cells. However, for the sake of experimental rigor, a direct experiment on real nerve cells is still needed to verify the effect of PNFF on nerve cells. The dorsal root ganglia neurons (DRGs) used in this experiment were derived from rats. β3-Tubulin is kind of neuron microtubule-associated proteins and a common neuronal maker. This protein is a common indicator of the growth of nerve cells for it relates to the axon migration and orientation. We conducted the immunofluorescence staining of three groups (i:Control, ii: PNFF No Excit, iii: PNFF Exict) of neurons(Figure 7d). The experimental results showed that β3-Tubulin was expressed in all three groups of experiments. However, the staining was most pronounced in the third group. The experimental results show that PNFF has a very good promoting effect on the growth of nerve cells under the condition of vibration.

To get direct evidence that PNFF stimulates neurons. we analyzed the distribution of the neuron microtubule-associated proteins Tuba1a and MAP2 and neuron growth related protein gene GAP43 in control and PNFF with excitation neurons (Figure 7e). The results show that: The expression of Tuba1a gene in the experimental group was 1.3 times that of the control group. The expression of GAP43 gene in the experimental group was 2.2 times that in the control group, and the expression of MAP 2 gene in the experimental group was 3.9 times that in the control group.

Through the above experiments, we systematically demonstrated that the electric charge generated by the multilayer film could stimulate the growth and differentiation of nerve cells through the nanofiber.

3. Conclusion

In this study, we prepared PLLA nanofibers by electrostatic spinning, and adjusted various parameters to improve their biological properties. At the same time, we prepared PLLA piezoelectric thin films by hot stretching and annealing. PLLA piezoelectric thin films and PLLA nanofibers were then pressed together using the hot-pressing method to prepare multilayer thin films. The experimental results showed that the voltage output performance of the multilayer film was slightly lower than that of the single piezoelectric film and higher than that of the single nanofiber film. Subsequently, we used this multilayer to grow neuron-like cells. The multilayer films were much better than single nanofibers or piezoelectric films in promoting cell-oriented growth. We experimentally proved that

this mode of piezoelectric stimulation activated calcium ion channels and increased the intracellular Ca^{2+} concentration. Additionally, By measuring the expression of important genes in nerve cells in different environments, it was confirmed that PNFF has a positive effect on stimulating nerve cell growth. Overall, because of the good performance of the PLLA multilayer films prepared, these piezoelectric multilayer materials have high potential in tissue engineering, particularly for electrically responsive tissue-like nerve cells.

4. Experimental Section

Fabrication of PLLA and PCL: As described in a previous article, PLLA nanofibers were fabricated using a conventional electrospinning (CES) method.[40] First, an appropriate PLLA solution, PLLA (molecular weight: 260 000; Daigang biomaterial, China), was dissolved in hexafluoro-isopropanol (HFIP) solvent (Aladdin, Shanghai, China) to make a 7.5% (w/t) PLLA solution. In addition, the PLLA solution was poured into a syringe, which was then placed on an injection pump (KDS101; KD Scientific, USA). The electrospinning speed was set at 0.5 ml h^{-1}, and a voltage of 12 KV/–3 KV was applied to the syringe needle (21 G) and rotating mandrel. Before spinning, a 2 cm-wide Al foil was attached to the rotating mandrel (800 rpm). The gap distance between the needle and mandrel was set to 20 cm. Next, a 7.5% PCL solution was prepared, by dissolving PCL (molecular weight of 240000; Daigang biomaterial, China) in a methylene chloride (Macklin Biochemical Co., Shanghai, China) solvent. Next, the PCL solution was loaded on the injection pump, and the same spinning conditions were applied to fabricate PCL NFs. Finally, in order to remove the residual solvent in PLLA and PCL nanofibers. The nanofibers should be kept warm for 10 h in a drying oven at 40 °C.

Fabrication of the PLLA Film: PLLA (0.8 g) was dissolved in 20 mL chloroform solvent (Macklin Biochemical Co., Shanghai, China), and the PLLA solution was stirred for one hour until the solution was completely dissolved. The solution was then poured into a special mold (10 cm × 10 cm) in a desiccator to dry for 24 h. The PLLA film was placed on the Lab-designed film stretching machine. The speeds of the front motor and rear motor of the film stretching machine were set to 0.08 and 0.02 mm min^{-1}, respectively. The temperature of the heating wire was set at 60 °C. The PLLA film was annealed in an incubator at 135 °C for 8 h. The annealed PLLA film was then cut into 3.5 cm squares, and hot-pressed together with the PLLA NFs using a hot-press machine at 55 °C.

The microstructure of the nanofibers was characterized by SU8020 scanning electron microscope (SEM). Nano Measure software was then used to evaluate the size distribution of the PLLA nanofibers. The hydrophilicity of the nanofibers was evaluated using a contact angle measuring instrument (OCA25; Data Physics Corporation, Germany). X-ray diffraction (XRD) was performed with a PANalytical X'Pert3 diffractometer (PANalytical Ltd., Netherlands) loaded a Cu Kα source with a step of 0.013° and a 2θ range from 10° to 50°. FTIR spectra were obtained using Vertex 80 V (Bruker Corp, MA, USA), and Fourier transform infrared spectroscopy was performed in the wavenumber range of 400–1600 cm^{-1} with a resolution of 4 cm^{-1}. The stress versus strain curve of the PLLA films was measured using a universal testing machine (Q800; TA Instruments Corporation, USA).

During the measurement of the piezoelectric coefficients, the force exerted on the PLLA multilayer nanofibers was measured using a load cell (ELPF-50N-C3006; Measurement Specialties Inc., VA, USA). The resulting electrical signal was measured using a phase-locked amplifier. (SR830; SRS, California, USA).

Biocompatibility Test: The Live/Dead and Cell Count Kit-8 (CCK-8) assays were used to evaluate the biocompatibility of the PNFF film. A calcein-AM/PI double-labeled kit (CA1630; Solarbio, China) was used to stain the live/dead PC-12 cells. The cells at 1, 3, and 5 days were gently washed three times using phosphate-buffered saline (PBS) solution to clear the external esterase activity. To stain the PC-12 cells at a density of $1 \times 10^{5-6}$ µL mL^{-1}, 1 µL mL^{-1} of calcein-AM and 3 µL mL^{-1} of PI

solution were added. Thereafter, 1X Assay Buffer (diluted to one-tenth the concentration of the original solution) was added, and the mixture was added to the PC-12 cells and incubated at 37 °C for 15 min. Next, the PC-12 cells were observed using an inverted fluorescence microscope (FSM) (DM6000; Leica, Germany) at a wavelength of 490 ±10 nm to view the live and dead cells at the same time and at a wavelength of 545 nm to view the dead cells only. For statistical analysis, five images of each group were chosen, and the proportions of live cells and dead cells were counted using ImageJ (National Institutes of Health, USA).

CCK-8 (CA1210, Solarbio, China) was also used to quantify cell viability. After removing the culture medium and washing the cells with PBS, a mixture of medium and CCK-8 (ratio: 10:1) solution was added to the PC-12 cells. Following incubation for 2 h, 200 µL of the culture supernatant was transferred to a 96-well plate, and the absorbance was measured at 450 nm using a microplate absorbance spectrophotometer (Bio-Rad Laboratories, Inc., Japan). For each of the groups, three wells were tested to ensure the correctness of the results (Figure 5).

Cell Culture and Differentiation: Cell differentiation was evaluated in PC-12 cells (ATCC CRL-1721). After culture to a stable stage, the PC-12 cells were collected and seeded on the PNFF scaffold and tissue culture polystyrene (TCPS; Corning Inc., USA) plates at a density of 6×10^4 cells ml^{-1}. The PC-12 cells were then cultured in Dulbecco's modified Eagle medium (Solarbio, China) containing 10% horse serum (HS; TMO, USA), 5% fetal bovine serum (FBS; TMO, USA), 100 IU/mL of penicillin, 100 µg mL^{-1} of streptomycin, and 2 mM L-glutamine. The cells were maintained at 37 °C in a saturated humidity atmosphere with 95% air and 5% CO$_2$. To study the differentiation of PC-12 cells, 50 ng mL^{-1} of nerve growth factor (NGF, Solarbio, China) was added to the cell medium to inhibit cell proliferation and generate long neurites in the PC-12 cells. Afterward, the cells were cultured on differentiation medium for five days for the next step.

Evaluation of the Cell Morphology: The cytoskeleton and nucleus were stained with Phalloidin (Proteintech, USA) and DAPI (Solarbio, China). The PC-12 cells of various groups after five days of electrical stimulation were assessed using the immunofluorescence staining method. First, PC-12 cells were fixed with paraformaldehyde (4%; Aladdin, Shanghai, China) for 20 min and washed three times with PBS. The cells were then permeabilized with Triton-X-100 (0.1%; Aladdin, Shanghai, China) for 10 min, washed three times with PBS again and stained with phalloidin (Proteintech, USA) for 40 min at room temperature. Finally, 4′,6-diamidino-2-phenylindole (DAPI; Solarbio, China) was added, and the PC-12 cells were stained for 10 min. The immunofluorescence staining images of cells were taken using a laser scanning confocal microscope (SP8; Leica, Germany). The directionality of the PC-12 nerve cell was measured by selecting five images of each group and measuring the sharp angles between the axon and horizontal direction in 20 different cells using ImageJ. The average neurite length and differentiation rate of PC-12 cells were also counted using the same method.

After five days of incubation of PC-12 cells on the PNFF film, the cells were fixed with 4% paraformaldehyde for 20 min and washed three times with PBS. Next, a series of ethanol solutions (15%, 30%, 50%, 60%, 70%, 80%, 90%, and 100%) were used to dehydrate the cells on the substrate at each concentration for 10 min. Before observation under electron microscopy, the films with cells were sputtered with gold for 40 s. Finally, SEM images of PC-12 cells were taken using a scanning electron microscope SU8020 SEM (Hitachi Ltd., Japan).

Measurement of Intracellular Calcium Levels and the Gene Expression of Neurons: To test the intracellular Ca^{2+} levels, the PC-12 cells were cultured and stimulated for five days, after which the cell medium was removed. Next, Hank's balanced salt solution (HBSS; Solarbio, China) was used to wash the cells three times, and then a working solution of Fluo 4-AM solution (Dojindo, Japan) was added to cover the cells. Next, the cells were incubated for 30 min at 37 °C. After removing the Fluo-4AM solution, the cells were washed with HBSS again three times and incubated for another 30 min with the HBSS solution. Finally, cell images were taken using a laser scanning confocal microscope at an excitation wavelength of 494 nm and an emission wavelength of 516 nm.

Dorsal root ganglia neurons (DRGs) were isolated from postnatal day 3 rat following a previously described procedure.[41] The culture medium is Neurobasal (Gibco, USA) with 2% B-27 (Gibco, USA) and 1% penicillin-streptomycin. All the culture medium was changed every two days. After culturing, DRGs were fixed in 4% paraformaldehyde for 30 min, permeabilized with 0.5% Triton X-100 solution for 5 min, and incubated with 10% goat serum (Solarbio, China) for 30 min at room temperature. Next, neurons were incubated with rabbit anti-beta III Tubulin antibodies (abcam, UK) at 4 °C overnight and then secondary antibodies with the goat anti-rabbit antibodies (IgG H+L, Alexa Fluor 594, Abcam, USA) for one hour in the dark at room temperature. After washing three times with PBS, the cells were observed via confocal laser scanning microscopy (SP8, Leica, Germany).

Total RNA of the cultured neurons in different groups were extracted and affinity purified with the FastPure Cell/Tissue Total RNA Isolation Kit (Vazyme, China). cDNA synthesis was performed using ≈10 ng of mRNA and HiScript® II Q Select RT SuperMix for qPCR (Vazyme, China). After mix the cDNA with Taq Pro Universal SYBR qPCR Master Mix (Q712, Vazyme, China), Real-time PCR was performed in triplicate with Real-time fluorescence quantitative PCR instrument (BIOER, China). Glyceraldehyde-3-phosphate dehydrogenase (GAPDH) served as an endogenous control (primer sequences and product sizes are listed in Table S2, Supporting Information). All the analyses were repeated in three independent experiments.

Supporting Information

Supporting Information is available from the Wiley Online Library or from the author.

Acknowledgements

Conflict of Interest

The authors declare no conflict of interest.

Data Availability Statement

The data that support the findings of this study are available in the supplementary material of this article.

Keywords

cell growth, multilayer film, nanofibers, piezoelectric film, PLLA

[1] R. Langer, J. P. Vacanti, *Science.* **1993**, *260*, 920.
[2] L. D. Jeanie, D. J. Mooney, *Biomaterials* **2003**, *24*, 4337.
[3] S. J. Hollister, *Nat. Mater.* **2005**, *4*, 518.
[4] Y. Shan, X. Cui, X. Chen, Z. Li, *Wiley Interdiscip Rev Nanomed Nanobiotechnol* **2023**, *15*, e01827.

[5] K. Kapat, Q. T. H. Shubhra, M. Zhou, *Adv. Funct. Mater.* **2020**, *30*, 1909045.

[6] G. Thrivikraman, S. K. Boda, B. Basu, *Biomaterials* **2018**, *150*, 60.

[7] Y. Zhao, Y. Liang, S. Ding, K. Zhang, H. Mao, Y. Yang, *Biomaterials* **2020**, *255*, 120164.

[8] W. Zhang, G. Li, B. Wang, Q. Zhu, L. Zeng, Z. Wen, C. Yang, Y. Pan, *Adv. Funct. Mater.* **2022**, *32*, 2203029.

[9] A. H. Rajabi, M. Jaffe, T. L. Arinzeh, *Acta Biomater.* **2015**, *24*, 12.

[10] C. Ribeiro, C. M. Costa, D. M. Correia, J. Nunes-Pereira, J. Oliveira, P. Martins, R. Goncalves, V. F. Cardoso, S. Lanceros-Mendez, *Nat. Protoc.* **2018**, *13*, 681.

[11] C. Ribeiro, M. S, V. Correia, J. G. Rocha, F. M. Gama, S. Lanceros-Méndez, *RSC Adv* **2012**, *2*, 11504.

[12] L. Ruan, X. Yao, Y. Chang, L. Zhou, G. Qin, X. Zhang, *Polymers (Basel)* **2018**, *10*, 228.

[13] S. Ribeiro, C. Puckert, C. Ribeiro, A. C. Gomes, M. J. Higgins, S Lanceros-Mendez, *ACS Appl. Mater. Interfaces* **2020**, *12*, 191.

[14] F. Fan, W. Tang, Z. L. Wang, *Adv. Mater.* **2016**, *28*, 4283.

[15] X. Chen, X. Li, J. Shao, N. An, H. Tian, C. Wang, T. Han, L. Wang, B. Lu, *Small* **2017**, *13*, 1604245.

[16] Y. M. Yousry, K. Yao, S. T. Chen, W. H. Liew, S. Ramakrishna, *Adv. Electron. Mater.* **2018**, *4*, 1700562.

[17] C. A. Silva, M. M. Fernandes, C. Ribeiro, S. Lanceros-Mendez, *Colloids Surf. B Biointerfaces* **2022**, *218*, 112708.

[18] R. A. Surmenev, T. Orlova, R. V. Chernozem, A. A. Ivanova, A. Bartasyte, S. Mathur, M. A. Surmeneva, *Nano Energy* **2019**, *62*, 475.

[19] A. Wang, Z. Liu, M. Hu, C. Wang, X. Zhang, B. Shi, Y. Fan, Y. Cui, Z. Li, K. Ren, *Nano Energy* **2018**, *43*, 63.

[20] M. Kitsara, A. Blanquer, G. Murillo, V. Humblot, S. De Braganca Vieira, C. Nogues, E. Ibanez, J. Esteve, L. Barrios, *Nanoscale* **2019**, *11*, 8906.

[21] R. Das, E. J. Curry, T. T. Le, G. Awale, Y. Liu, S. Li, J. Contreras, C. Bednarz, J. Millender, X. Xin, D. Rowe, S. Emadi, K. W. H. Lo, T. D. Nguyen, *Nano Energy* **2020**, *76*, 105028.

[22] B. Xia, Y. Lv, *Mater. Sci. Eng. C Mater. Biol. Appl* **2018**, *82*, 253.

[23] A. R. D'Amato, D. L. Puhl, A. M. Ziemba, C. D. L. Johnson, J. Doedee, J. Bao, R. J. Gilbert, *PLoS One* **2019**, *14*, 0211731.

[24] G. Zhao, B. Huang, J. Zhang, A. Wang, K. Ren, Z. L. Wang, *Macromol. Mater. Eng.* **2017**, *302*, 1600476.

[25] X. Du, C. Zhao, J. Zhang, K. Ren, *J. Appl. Phys.* **2016**, *120*, 164101.

[26] X. Zong, K. Kwangsok, D. Fang, S. Ran, S. H. Benjamin, B. Chu, *Kobunja Kwahak Kwa Kisul* **2002**, *43*, 4403.

[27] S. H. Tan, I. R, K, M, S. Ramakrishna, *Kobunja Kwahak Kwa Kisul* **2005**, *46*, 6128.

[28] E. A. Vogler, *Adv. Colloid Interface Sci.* **1998**, *74*, 69.

[29] Y. Wang, J. Zhang, B. Zhang, K. Ren, *Macromol. Mater. Eng.* **2021**, *306*, 2100402.

[30] J. F. TurnerII, A. Riga, A. O'Connor, J. Zhang, J. Collis, *J. Therm. Anal. Calorim.* **2004**, *75*, 257.

[31] A. C. Renouf-Glauser, J. Rose, D. F. Farrar, R. E. Cameron, *Biomaterials* **2005**, *26*, 5771.

[32] K. Jong, H. Wang, B. Jin, *Eur. Polym. J.* **2001**, *37*, 907.

[33] O. Tsutomu, E. Fukada, *Jpn. J. Appl. Phys.* **1998**, *37*, 3374.

[34] A. Merlo, V. Mokkapati, S. Pandit, I. Mijakovic, *Biomater. Sci.* **2018**, *6*, 2298.

[35] D. F. Williams, *Biomaterials* **2008**, *29*, 2941.

[36] S. Ma, H. Liu, H. Jiao, L. Wang, L. Chen, J. Liang, M. Zhao, X. Zhang, *Neurotoxicology* **2012**, *33*, 59.

[37] A. Chen, X. Lai, H. Liang, Y. Zhang, Y. Kang, Y. Lin, L. Shao, *Nanomedicine* **2018**, *13*, 1067.

[38] M. J. Berridge, M. D. Bootman, P. Lipp, *Nature* **1998**, *395*, 645.

[39] X. C. M. Hoop, A. Ferrari, F. Mushtaq, G. Ghazaryan, T. Tervoort, D. Poulikakos, B. Nelson, S. Pané, *Sci. Rep.* **2017**, *7*, 4028.

[40] J. Zhang, S. Gong, C. Wang, D. Y. Jeong, Z. L. Wang, K. Ren, *Macromol. Mater. Eng.* **2019**, *304*, 1900259.

[41] H. Shen, M. Gan, H. Yang, J. Zou, *J Int Med Res* **2019**, *47*, 3253.